World Academy of Science, Engineering and Technology
International Journal of Energy and Power Engineering
Vol:17, No:5, 2023

Supervisory Controller with Three-State Energy Saving Mode for Induction Motor in Fluid Transportation

O. S. Ebrahim, K. O. Shawky, M. O. Ebrahim, P. K. Jain

***Abstract*—**Induction Motor (IM) driving pump is the main consumer of electricity in a typical fluid transportation system (FTS). Changing the connection of the stator windings from delta to star at no load can achieve noticeable active and reactive energy savings. This paper proposes a supervisory hysteresis liquid-level control with three-state energy saving mode (ESM) for IM in FTS including storage tank. The IM pump drive comprises modified star/delta switch and hydromantic coupler. Three-state ESM is defined, along with the normal running, and named analog to computer ESMs as follows: Sleeping mode in which the motor runs at no load with delta stator connection, hibernate mode in which the motor runs at no load with a star connection, and motor shutdown is the third energy saver mode. A logic flow-chart is synthesized to select the motor state at no-load for best energetic cost reduction, considering the motor thermal capacity used. An artificial neural network (ANN) state estimator, based on the recurrent architecture, is constructed and learned in order to provide fault-tolerant capability for the supervisory controller. Sequential test of Wald is used for sensor fault detection. Theoretical analysis, preliminary experimental testing and, computer simulations are performed to show the effectiveness of the proposed control in terms of reliability, power quality and energy/coenergy cost reduction with the suggestion of power factor correction.

***Keywords*—**Artificial Neural Network, ANN, Energy Saving Mode, ESM, Induction Motor, IM, star/delta switch, supervisory control, fluid transportation, reliability, power quality.

I. Introduction

THE use of cybernetic computing and information through Web has become a common approach to modern optimal control and management. Thanks to the advances of Internet of Things (IoT) technology, many social and industrial Web-based cybernetic applications are now feasible such as; medical diagnosis, information services, smart meters and billing, building and factory management, transportation control, and many other opportunities.

Fig. 1 shows generic block diagram of an FTS connected to a computer-cyber via internet. The computer-cyber receives massive information from the plant's sensors, controllers, and users. Then, it performs complicated data manipulations and mathematical programming, considering various factors and physical constraints, in order to achieve optimal system management in terms of global impacts such as; reliability, service quality, power quality and, load demand satisfaction at attractive energetic cost etc. Accordingly, the decisions of localized public (supervisory) control have to be linked, by way of design and objective, to these global impacts [1], [2].

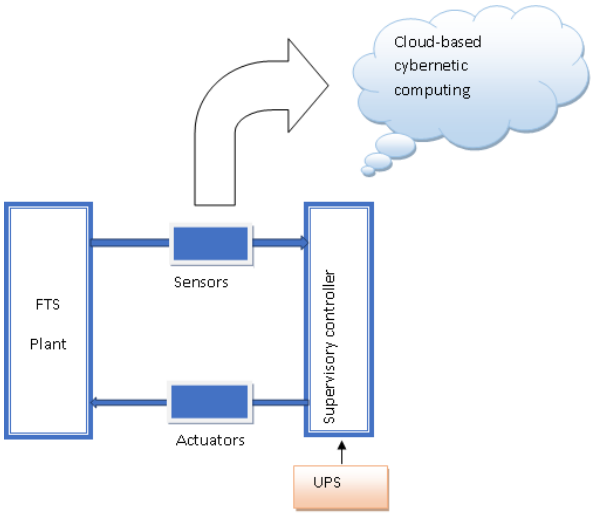

Fig. 1 Generic Blok Diagram of an FTS connected to Internet

In a typical FTS, IMs driving pumps are the main consumers of electricity and most of them are squirrel cage. These motors are cheap, robust and relatively straightforward to operate. However, some precautions have to be taken due to high starting current. It can cause voltage dips and thermal overload which are problematic for the end users of the same power network and for the motor itself. Those problems can be alleviated by choosing suitable motor starting method and appropriate power supply connection [3]. Fig. 1 shows an uninterruptable power supply (UPS) feeding critical (control and protection) system components with electricity in order to make them insensitive to electrical grid disturbances [3], [4].

More often than not, the FTS process optimization requires hydraulic tank, acting as energy storage element or load shifter, to achieve cost reduction without violating the service quality [5], [6]. Therefore, the component's efficiency rather than the pump affinity law is the factor for energy saving assessment. Fig. 2 (a) shows a hydraulic storage tank having

O. S. Ebrahim, Ph.D., is with the Dept. of Electrical Power and Machines, Faculty of Engineering, Ain Shams University, Egypt (e-mail: osama.shawky@eng.asu.edu.eg).

K. O. Shawky is a student at the Civil Dept., Faculty of Engineering, Ain Shams University, Egypt (e-mail: kareem.osama@eng.asu.edu.eg).

M. O. S. Ebrahim is a student at the Faculty of Commerce, Ain Shams University, Egypt.

P. K. Jain, Prof., is the Director of ePOWER Research Center, Queen's University, Ontario, Canada (e-mail: praveen.jain@queensu.ca).

input flow rate, q_i, and load flow, q_0, independent of the liquid level, h, or head. The governing dynamic equation is given by (1) where, A is the tank cross-section area.

$$\tilde{h}\,(t) = \frac{1}{A}\int (q_i - q_0)dt \tag{1}$$

The cybernetic computer generates the head command h^* which satisfies the optimization problem over a specific time interval. The supervisory controller achieves this command using on-off control or hysteresis control. Hysteretic controller offers high robustness against un modeled dynamics and ease of implementation (for instance, tank with variable cross section area) and its adaptive version can resemble the deadbeat control [6]. However, (1) represents a pure integrator that is sensitive to sensor noise and DC offsets [7], [8]. Therefore, online estimation of the liquid-level for fault tolerant control capability (i.e., the ability of controller to operate with satisfactory performance under sensor defects) is problematic especially; q_i and q_o are normally slow time-varying quantities.

In order to overcome these difficulties, this paper exploits the full controllability and thermal capability of a motor pump drive FTS comprising; IM, modified star/delta starter, hydromatic (fluid) coupling, centrifugal pump and a storage tank. Three motor states, during inflow off period, are distinguished and introduced. A logic flow-chart is constructed to select the best motor state for active and reactive energy cost reduction considering the motor thermal information. Further, recurrent neural network (RNN) state estimator is proposed in order to provide fault-tolerant ability and enhance the reliability of the proposed control. In the followings, this scheme will be illustrated and introduced.

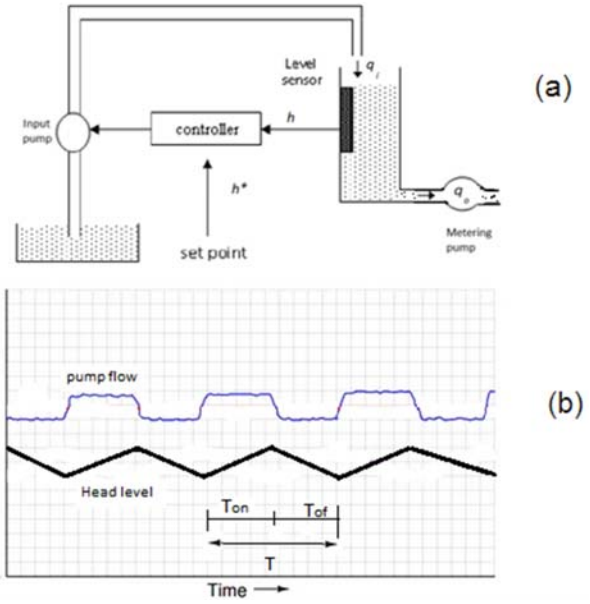

Fig. 2 Storage tank control (a) and plot of input flow and liquid-level (b)

II. RNN-Based Supervisory Controller

A. Hysteresis Liquid-Level Control

Hysteresis control as in Fig. 2 is a simple method of controlling the tank liquid level. The main principle is based on direct pumping of liquid such that its level or head h approximates its reference value h^* in average sense. The hysteresis block in Fig. 2 (a) compares the difference between h^* and h with a defined band, Δ, as:

$$\begin{cases} 1 & h^* - h > \Delta \\ nochange & -\Delta < h^* - h < \Delta \\ 0 & h^* - h < -\Delta \end{cases} \tag{2}$$

The pump on-off operation depends on whether the measured head reaches the upper or lower value of the hysteresis. Fig. 2 (b) demonstrates an example for the liquid level and pump flow at steady state.

B. Recurrent NN Estimator

For fault-tolerant ability, the measured head h is replaced by its estimate value $\tilde{h}$ in the feedback control loop. The problem of pure integrator windup in (1) is cured by proposing full state estimator based on feedforward neural network with recurrent structure (RNN) as shown in Fig. 3. The RNN has one input layer, one hidden layer, one output layer, and biasing source. The input and output layer neurons dictated by the number of respective signals and the hidden layer neurons with sigmoid activation function. The synthesized RNN configuration has noise immunity and dynamic processing ability. Since the number of input neurons exceeds what is necessary to determine the output pattern, i.e. over-determined or redundant NN, it can work after training with one (or two) of its input neurons inhabited. This is similar to the case if one (or two) of the plant sensors is defected.

The fault-tolerant ability of the proposed RNN state estimator has the potential to improve the overall availability of the sensing elements. To demonstrate this, we assume that q_o, q_i, and h sensors have availability A of 80% each. The resultant availability of the RNN estimator will be

$$[1-(1-A_1A_2)(1-A_3A_2)(1-A_1A_3)] = 1 - 0.36 * 0.36 * 0.36 = 95.3344\ \%.$$

Furthermore, if the load flow q_o is dependent variable or its profile is known, the RNN can work as a best fit estimator with two sensors defected, i.e., two out of three sensors, which increases the overall availability to

$$[1-(1-A_1)(1-A_2)(1-A_3)] = 1 - 0.2 * 0.2 * 0.2 = 99.2\ \%.$$

Here, we assume that the availability of microprocessor-based data acquisition card = 100% where, availability A = 1-failure rate.

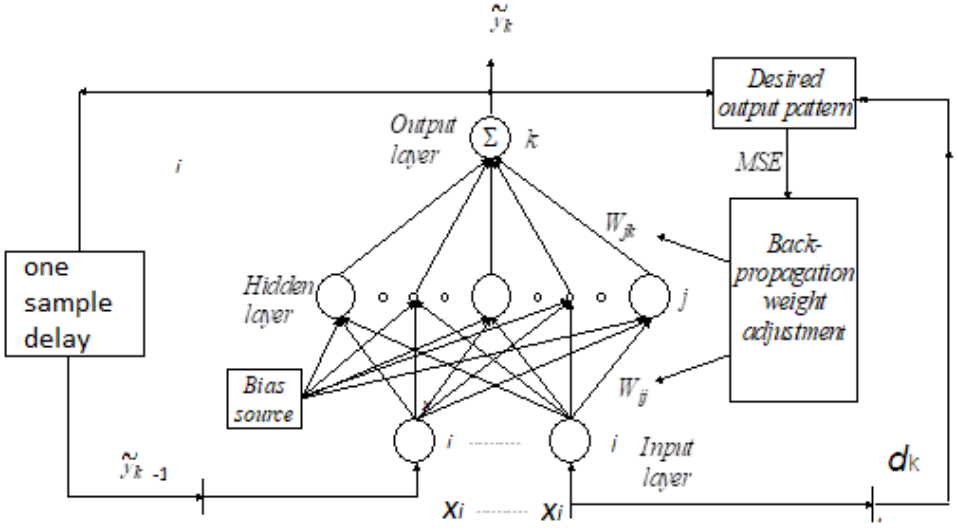

Fig. 3 Three-layer feedforward RNN

We consider that the RNN is being trained. The training data comprise q_o, q_i, and h measurement information as input as well as desired pattern and their corresponding estimate as output pattern. We consider that the network is being trained by the input pattern n, the weights and biases of the network are updated using the back-propagation technique to minimize the network performance function. A common performance function for the feedforward networks is the mean squared error *MSE*.

$$MSE = \frac{1}{Q}\sum_{k=1}^{Q}(d_k^n - \widetilde{y_k^n})^2 \tag{3}$$

Where $\widetilde{y_k^n}$ = output of the k^{th} neuron in the output layer, d_k^n = corresponding desired output, and Q = dimension of the output vector (in our case Q = 3). The weights of the neurons are altered to minimize the value of *MSE* by gradient descent method. The weight update equation is then given as

$$W_{ij}(l+1) = W_{ij}(l) - \eta \frac{\partial MSE}{\partial W_{ij}(l)}. \tag{4}$$

where η = learning rate, $W_{ij}(l+1)$ = new weight between i^{th} and j^{th} neurons, and $W_{ij}(l)$ = corresponding old weight. The weights are iteratively updated and a momentum term $\beta[W_{ij}(l+1) - W_{ij}(l)]$ is usually added to the right-hand side of (4), where β is a small value, in order to improve training performance [9], [10].

C. Data Conditioning and Fault Detection

For RNN training, measurement sets of tank variables shall be collected online during periodic phases of data acquisition. An averaged signal for each channel is computed and considered as a reference pattern. Cross correlation between coefficients of single samples and the averaged pattern are calculated. The samples with very low correlation coefficients are discarded. Fig. 4 (a) demonstrates simulated time response (using MATLAB/Simulink) of RNN based estimator for the pump outflow during training, testing, and validation phases using input signal with white noise. Fig. 4 (b) shows the samples autocorrelation-error curve and the corresponding level of confidence.

The confidence limit is similarly determined for sensor fault detection using Wald's likelihood ratio test. The method is based on choosing between two hypothesis H_0 (normal behavior) and H_1 (abnormal behavior) according to signal signature [11]. For each error signal $E_k(t)$, we define $P(E_k^J/H_o)$ and $P(E_k^J/H_1)$ as a priori density probability where E_k^J is a vector of J samples of the signal $E_k(t)$. The likelihood ratio is given by

$$\gamma_k = \frac{P(E_k^J/H_o)}{P(E_k^J/H_1)} = \prod_{i=1}^{J}\frac{P(E_k^i/H_o)}{P(E_k^i/H_1)} \tag{5}$$

Then the formulation of Wald test is given by (6):

$$\begin{cases} normal & A > \gamma_k \\ no\ decision & A < \gamma_k < B \\ abnormal & B < \gamma_k \end{cases} \tag{6}$$

where A = $P_{MF}/(1-P_{RA})$ and B = $(1-P_{MF})/P_{RA}$ with P_{MF} is the probability to miss faulty measurement and P_{RA} is the probability of wrong alarm.

Wald's test for sensor fault detection can be formulated in terms of significant deviation of the reference mean value μ assuming that $P(E_k^J/H_o)$ and $P(E_k^J/H_1)$ are Gaussian:

$$\begin{cases} normal & \sum_{i=1}^{J} V_i < T_o \\ no\ decision & T_o < \sum_{i=1}^{J} V_i < T_1 \\ abnormal & \sum_{i=1}^{J} V_i > T_1 \end{cases} \tag{7}$$

The two test frontiers are as in (8):

$$T_0 = \frac{\sigma^2 lnA}{\mu_0 - \mu_1} \& T_1 = \frac{\sigma^2 lnB}{\mu_0 - \mu_1} \tag{8}$$

and

$$V_i = E_i - \frac{J(\mu_0 - \mu_1)}{2} \quad (9)$$

Here, we assume that the mean value μ_o and the variance σ^2 are determined during training phase using sensor data-sheet and μ_1 is the increase (or decrease) in μ checking in which the sensor fault detector will be triggered as illustrated on Fig. 5 (a). Consequently, the output of Wald's test will inhabit the defected sensor signal and the corresponding input neuron will be assigned to its delayed estimate signal as depicted schematically in Fig. 5 (b). Further, Wald's test can be repeated more than once (analog to the automatic circuit recloser operational sequence) in order to discriminate between temporary/transient and permanent sensor failures.

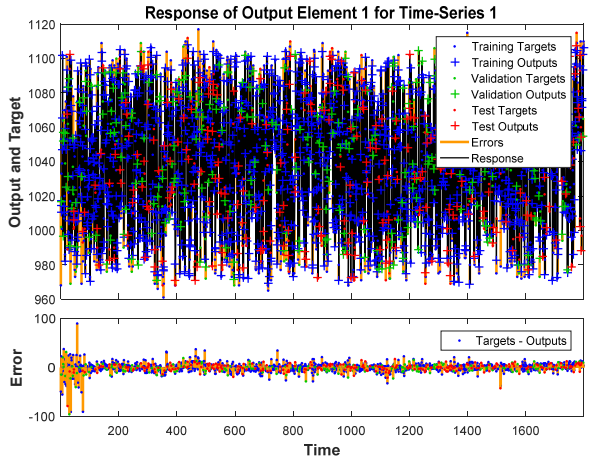

(a)

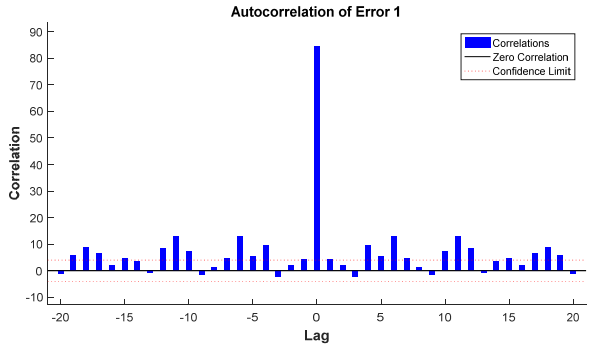

(b)

Fig. 4 Time response of the RNN (a) and Autocorrelation-error curve (b)

III. IM Drive

A. Modified Star/Delta Starter

Recent recommendations and regulations to replace standard and high efficiency class motors with premium and super-premium ones make IM a viable choice for FTS gross cost reduction [12]. However, the higher the IM efficiency is, the higher its inrush starting current will be. The state-of-the-art electronic voltage source inverter can yield excellent dynamic speed response by varying the motor frequency but; it is not economical to be used as a starter only [9]. Therefore, in applications such as on-off controlled IM pump, where dynamically varying the operating speed is less important than pump startup, stopping, and drive train isolation, the combination of electromechanical start/delta starter with hydromatic (fluid) coupling as shown in Fig. 6 represents a good fit [13], [14]. Such a drive is controllable and enable the motor to be rated on running rather than starting torque.

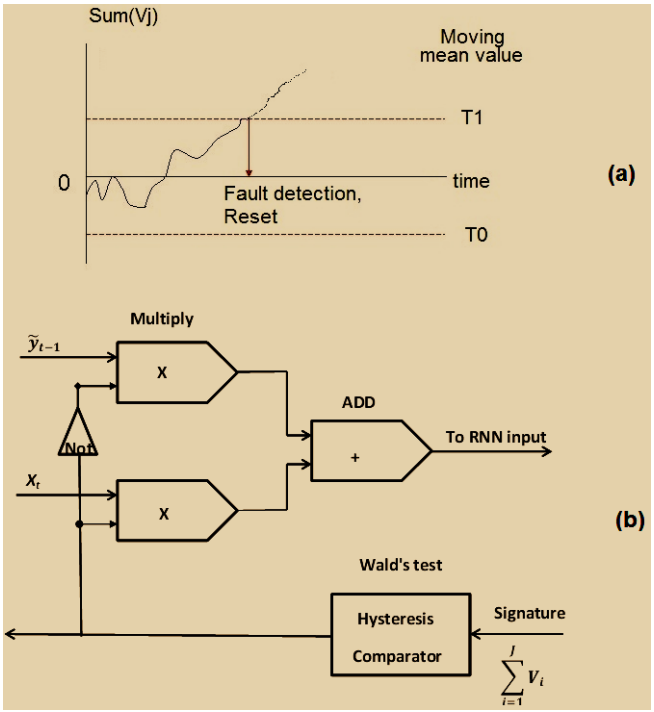

Fig. 5 Mean value, boundaries, and sensor fault detection (a) and circuit-diagram of defected signal replacement (b) [17]

The motor starts at no load with star connected stator windings, reducing the starting current and torque to one third of their nominal values. When the motor speed approaches the synchronous speed ω_1, the stator connection is changed to delta. Then, the hydromatic coupler gradually starts to load the motor by gradual coupling of the pump shaft to motor shaft. Mechanical clutches that operate too early or too suddenly will also produce severe current peaks. But current surges may occur for another reason even when care is taken to avoid premature operation of a change over switch. In fact, any starting method that involves a momentary disconnection of the supply main (such as; autotransformer and star/delta switch) may cause transient current surges of a very severe nature due to remaining voltages across its terminals that decay gradually in the temporarily open circuited stator windings. When the star switch is now closed in delta position, the supply voltages are reconnected to stator windings which have induced EMFs of comparable size but with a relative time shift that may be anything between coincidence and opposition. In the former case, there will be a very large current surge in all phases and possibly reinforced

by the magnetic saturation effect.

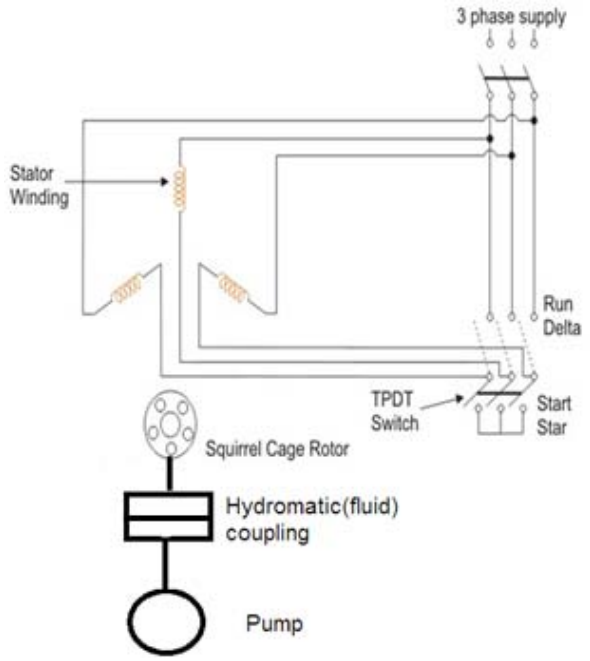

Fig. 6 IM drive with star/delta starter and hydromatic coupler

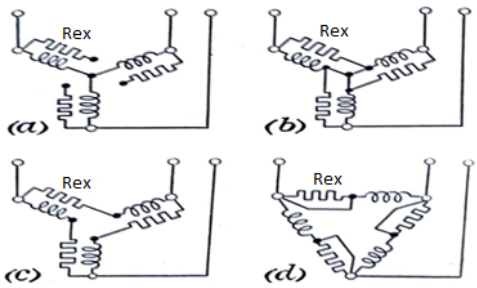

Fig. 7 Modified star/delta starter sequence of operation [14]

To avoid these current surges, a modified star/delta starter is used here to maintain the connection between stator and supply line, by inserting an external resistance, while changeover is made [14]. The sequence of modified star/delta operation is shown in Fig. 7. The motor is switched on in star (a), resistors are paralleled with the phases (b) leaving the motor itself unaffected; the motor star point is opened (c) putting the windings in delta with series resistance; and (d) the resistors are short-circuited. The method is limited to normally delta connected motors up to 3000 V, since high voltage motors are usually star connected.

B. Three-State ESM

By considering the full controllability of the proposed drive, three possible states for the motor during inflow off period (T_{off}) can be discriminated. They are named, analog to the popularly used computer's ESMs as they have same off-time characteristics, as follows:

1. Sleeping Mode

The motor is decoupled from the pump shaft and runs at no load with delta connected stator windings. The active and reactive energy consumptions are given by;

$$W_{nl\Delta} \approx \frac{3V_1^2}{R_c} T_{off} \& Q_{nl\Delta} \approx \frac{3V_1^2}{X_m} T_{off} \quad (10)$$

where V_1, R_c and X_m respectively are the per phase nominal voltage, no load resistance and, magnetizing reactance. Thanks to the fluid coupler, this mode of operation achieves remarkable energy savings compared with preventing the pump flow using throttling valve.

2. Hibernate Mode

The motor runs at no load with its terminals star connected. The energy consumption will be reduced to one third of (10) assuming linear magnetic circuit, i.e.

$$W_{nlY} \approx \frac{3(V_1/\sqrt{3})^2}{R_c} T_{off} \& Q_{nlY} \approx \frac{3(V_1/\sqrt{3})^2}{X_m} T_{off} \quad (11)$$

However, the motor-pump system in this mode takes longer time to re-operate at full load than the sleeping mode.

3. Shutdown Mode

The motor is disconnected from the grid supply and consumes no active and reactive power. However, it loses the kinetic energy $\frac{1}{2}J\omega_1^2$ stored in its moment of inertia J. For restarting, the motor will dissipate amount of energy equals $\frac{1}{2}J\omega_1^2$ as a heat in the rotor resistance, r_2, and equals $(\frac{r_1}{r_2})\frac{1}{2}J\omega_1^2$ as a heat in the stator resistance, r_1, (see Appendix A). Assuming $r_1 = r_2$, the total active and reactive energy consumptions associated with the shutdown decision, W_{sh} and Q_{sh} respectively, are

$$W_{Sh.D} = 1.5J\omega_1^2 \quad \& Q_{sh.D} = W_{Sh.D}\tan(\varphi_{st}) \quad (12)$$

where, φ_{st} is the motor phase angle at starting.

C. Thermal Capacity Used

Fundamentally, digital thermal overload protection works of the I^2t principle and derived from the temperature and time solutions of the first order thermal model [15].

$$\frac{d\theta}{dt} = \frac{1}{\tau}(\theta_f - \theta) \quad (13)$$

where $\theta, \theta_f,$ and τ respectively are temperature-rise (above ambient), final temperature-rise (above ambient), and thermal time constant. The recursive temperature solution to (13) is given in (14):

$$\theta_n = \theta_{n-1} + (\theta_f - \theta_{n-1})(1 - e^{-\frac{\Delta t}{\tau}}) \quad (14)$$

where θ_n, θ_{n-1}, and, Δt respectively are the calculated present temperature, temperature at previous time step and time step between calculations. Further, $\theta_f = (I/I_{ref})^2 T_{ref}$ where I, I_{ref}, and T_{ref} respectively are the motor phase current, set current

reference, and set temperature rise reference. Thermal Capacity Used (TCU) is calculated based on rated motor current with an overload factor applied and expressed as a percentage of maximum temperature. The thermal protection trips when TCU reaches 100%.

Calculation of the time to reach a specified temperature θ based on load and preload temperature is given by

$$t = \tau \ln\left(\frac{\theta_f - \theta_o}{\theta_f - \theta}\right) \quad (15)$$

The advantage of using thermal protection instead of over-current protection is that it has thermal memory (counter). This is critically important in the event of repetitive overload (starting) where, missing the motor thermal information could lead to numerous problems such as insulation failure. On the other hand, imposing the maximum permissible number of consecutive start/hr as a constraint in the FTS optimization problem adds difficulty and reduces the effectiveness of the solution. This is because the permissible number of consecutive cold start/hr is different from the permissible number of consecutive hot start/hr.

In the followings, we will construct a logic flow chart that relax this burden up to scale it becomes useful even for the human operators.

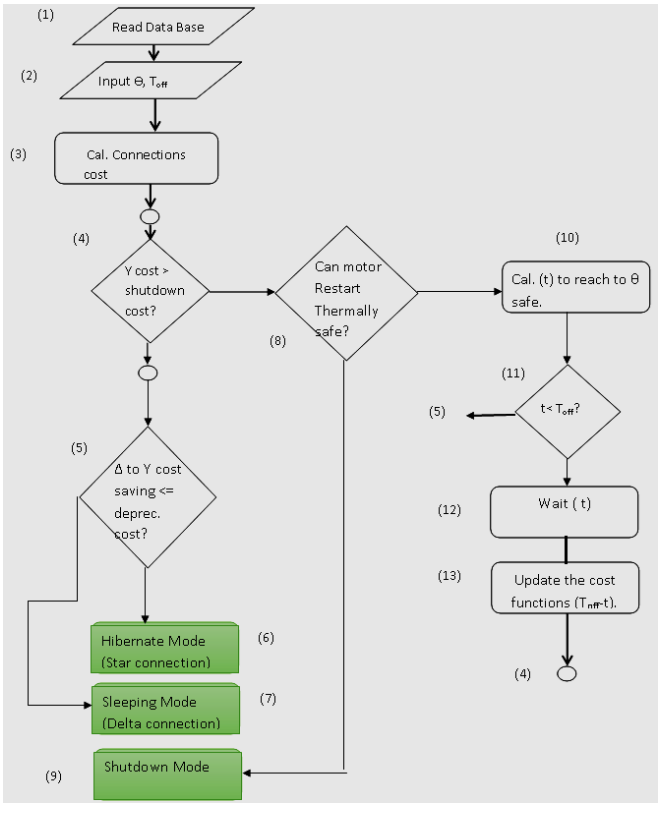

Fig. 8 Three-state ESM Logic selector

IV. Logic Flow Chart

A logic flow chart is synthesized to select the least expensive motor state during inflow off period (T_{off}), based on the following assumptions:

i) The distribution system feeding the motor and the motor branch circuit are not poorly designed such that starting of an IM using star/delta starter can lead to supply interruption (i.e., comply with NEC430-52 standard).

ii) In deregulated electricity market with the suggestion of power quality market, we expect using suitable meters and tariff structure such that the customers are paying for their emission of electrical disturbances and harmonics into the distribution network. These emissions may be caused by excessive reactive power consumption during IM starting or harmonic currents generated by electronic source inverter with input diode bridge rectifier. In such a way, these customers are encouraged to install power factor correction (PFC) or harmonic filter to mitigate their power quality problems [3], [14], [16].

iii) The load profile is known; such that the variations of hysteric control period ($T=T_{on}+T_{off}$) due to operating point changes can be compensated.

The procedure consists of the following steps shown in Fig. 8:

Step1. Read the data base file. The following data must be supplied: motor thermal rates, cost of 1 kWh, cost of 1 kVARh and any power quality (PQ) indices if exist, no-load active and reactive losses.

Step2. Input the motor temperature θ and T_{off} period.

Step3. Calculate the costs of motor being delta or star connected during T_{off} from (10) and (11), cost of shutdown from (12), and any existing PQ index term, and the depreciation cost of star/delta starter. The depreciation cost is calculated based on the gross cost of star/delta starter divided by its expected number of switching operations before failure (typically 500,000-1000,0000 times).

Step4. If the star connection cost is greater than shutdown cost, go to step8.

Step5. If the cost difference between delta and star connections is less than or equal to the depreciation cost, go to step7.

Step6. Change the motor connection to star (hibernate mode).

Step7. Remain the motor delta connected (sleeping mode).

Step8. If θ is greater than θ_{safe} go to step10. The safe temperature-rise θ_{safe} is calculated using starting current ratio and the acceleration time.

Step9. Shutdown mode.

Step10. Calculate the time (t) needed to reach θ_{safe} from (15).

Step11. If (t) is less than (T_{off}) go to step12else go to step5.

Step12. Wait time (t) to cool the motor to θ_{safe}.

Step13. Update the cost functions in terms of (T_{off}-t).

Step14. Go to step4.

A counter can be added to the mode decision blocks in order to calculate the expected life-time of star/delta switch and the time to maintain. In addition to use of mechanically interlocked switches, these have the potential to improve the starter reliability.

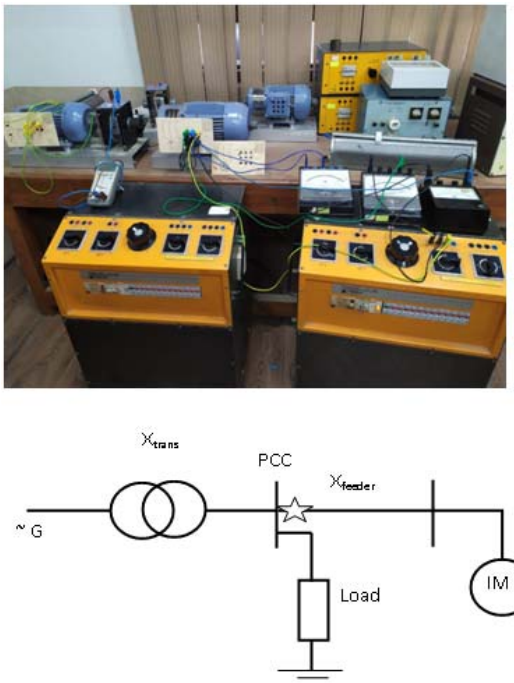

Fig. 9 IM Testing setup (a) and radial distribution system feeding the motor with marked location for PFC (b)

V. Cost Analysis

Preliminary testing has been carried out on a 3-phase, 50 Hz, 4-poles, 240 V, delta-connected IM using a laboratory setup shown in Fig. 9 (a). The objective of the tests is to determine the various motor characteristics required for the logic flow ESM selector (such as; no load active and reactive power losses, per unit starting current, rotor and stator resistances, moment of inertia, motor thermal rates, etc.) considering the following conditions: ambient temp. $\Theta_{amb} = 30$ °C, Trip temp. $\Theta_{Trip} = 90$ °C (Y class of insulation), and safe temp. for restarting $\Theta_{safe} = 70$ °C.

Furthermore, a radial distribution system as shown in Fig. 9 (b) is assumed to supply the motor and emulated in the Lab. Where the reactance of the transformer and motor feeder is 4.3% of the motor KVA base, starting current = 3.2 pu, and acceleration time ≈ 4 s. The IEEE definition of voltage dip at the point of common coupling (PCC) is considered as a sudden reduction of the voltage followed by recovery after a period of time from half cycle to one minute over 10% and less than 100%. Here, we put a PQ penalty of 1% pu cost for each voltage dip occurrence due to motor shutdown and restarting that is over 10% and less than 20%.

A per unit cost analysis is performed assuming the following factors; $C_e = 1$ pu, $C_Q = 0.4$, and T = 30 minutes, respectively, are the cost of 1 kWh, cost of 1 kVARh, and the optimization control period.

The results of the cost analysis are shown in Fig. 10 with and without PFC method installed at the upstream feeder end, respectively, indicated by the upper and lower curve. The relative cost saving is calculated w.r.t. the throttling cost.

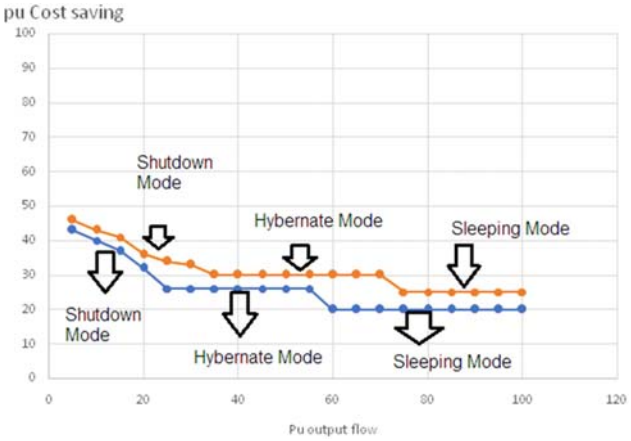

Fig. 10 Percent cost saving as a function of % output flow at constant head

The throttling power losses are emulated in the Lab. as a brake during the temperature-rise test which is carried out using two identical IMs connected to the same shaft. The first motor (the driving one) runs at rated positive sequence voltages while, the second motor is supplied by a reduced negative sequence voltages and rotates as a brake against its rotating field. In that test, the temperature-rise curves of the driven motor (brake) are determined, as well; the throttling power losses are approximated to the input powers to the driving machine. Fig. 10 shows noticeable effects of delta/star transition on pu cost savings at medium flow rates. The reduction of cost savings by using restrictive tariff structure (blue curve) can be justified, from the utility point of view, by limiting the electric voltage disturbances due to repetitive starting and as a motivation for using reactive power compensation method (red curve). Therefore, the parameter CQ in the cost analysis is assigned a value of 0.4 which is greater than the typical cost of a capacitive compensator/ KVAR. Consequently, with higher penalty on voltage sag, the shutdown mode will disappear and hibernate mode will be extended to the low flow region. The cost difference indicates that more cost reduction at low flow rates can be achieved by using, either a) switched capacitor VAR compensator or b) a low-rated (25-30%); efficiency optimized; inverter-fed; pumping beside to the main pumping units [9], [17].

VI. Conclusion

This paper introduced a three-state ESM and logic selector for on-off controlled IM drive with modified star/delta switch and fluid coupler. The procedure implements the motor thermal information and grid-compatible tariff structure. This has the potential to alleviate burden on the FTS optimization and PQ concern. Furthermore, the paper proposed a hysteresis liquid-level controller with fault-tolerant ability using state estimator based on the RNN configuration. Wald's likelihood ratio method is adopted for sensor fault detection. Computer simulations and theoretical analysis on a laboratory IM setup have been conducted and the results showed the validity and effectiveness of the introduced and effectiveness of the

introduced control and ESM logic selector.

APPENDIX

The motor acceleration-time under pure inertia loads can be calculated from the dynamics of rotating mass as follows

$$M = J\frac{d\omega_r}{dt} \tag{16}$$

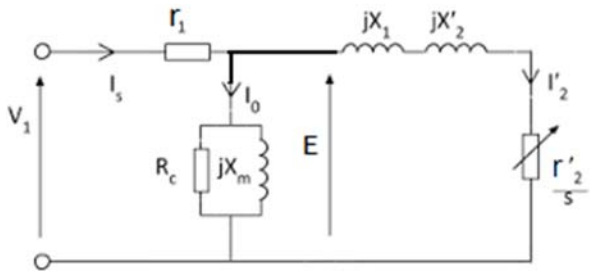

Fig. 11 An equivalent circuit for IM

where *J, M,* and, ω_r respectively are the motor inertia, motor torque and rotor angular speed. From the IM equivalent circuit shown in Fig. 11, the motor torque is related to the maximum torque by

$$\frac{M}{M_m} = 2/[(\frac{s}{\alpha}+\frac{\alpha}{s})]\ ; \tag{17}$$

where $s = \omega_1\text{-}\omega_r/\omega_1$ and $\alpha = r_2'/(x_1+x_2')$ respectively are the slip and the slip for maximum torque. Now from (16),

$$\frac{M}{M_m} = \frac{J\omega_1}{M_m}.\frac{d}{dt}\left(\frac{\omega_r}{\omega_1}\right) = \frac{-J\omega_1}{M_m}\frac{ds}{dt} \tag{18}$$

Combining the two expressions, yields

$$dt = \frac{-J\omega_1}{2M_m}(\frac{s}{\alpha}+\frac{\alpha}{s})ds \tag{19}$$

which for acceleration from standstill to slip *s* gives

$$t = \frac{J\omega_1}{2M_m}(\frac{1-s^2}{4\alpha}+\frac{\alpha}{2}ln\frac{1}{s}) \tag{20}$$

For s = 0.1;

$$t_{acc} \approx \frac{J\omega_1}{2M_m}(\frac{0.25}{\alpha}+1.15\alpha) \tag{21}$$

Rotor Heating: The current equation can be arranged to give $I_2 = E/\sqrt{(x_1+x_2')^2+(r_s'/s)^2}$ or $I_2 \approx I_{st}/\sqrt{1+(\alpha/s)^2}$

The rotor heat loss is $\int I_2^2 r_2 dt$ joules per phase which from (19) for a pure inertia load start is $W_{r_2} = -\frac{I_{st}^2 r_2 J\omega_1}{2\alpha M_m}\int sds = \frac{I_{st}^2 r_2 J\omega_1}{2\propto M_m}.\frac{1-s^2}{2}$. During acceleration from s = 1 to negligible slip, the rotor heat is therefore; $I_{st}^2 r_2 J\omega_1/4\alpha M_m$ joules per phase. Now the maximum torque in synchronous watts is 0.5 E I_{st} per phase, and $\alpha = I_{st}r_2/E$; so that W_{r2} reduces quite simply to $0.5J\omega_1^2$, identical with the kinetic energy that has been stored in the rotating parts. The heat loss W_{r2} is unavoidable and the only way to reduce this loss is to transfer part of it to an external resistance in case of slip ring motors.

Stator Heating: A heat loss comprising $(r_1/r_2)W_{r2}$ will be consumed in the stator resistance r_1.

ACKNOWLEDGMENT

We are sincerely grateful to Prof. M. A. Badr, Vice president of the Future University, Cairo, Egypt and the reviewers for their useful suggestions to revise the paper.

The authors would like to thank the reviewers for their constructive comments and people who helped them during writing phase of this work.

REFERENCES

[1] H. B. (Teddy) Pŭttgen, "R&D in our industry: where do you go from here?" Inter. Conf. on power system technology, Powercon2004, Keynote Address, pp.9, Singapore, 2004.

[2] S.M. Kaviri, H. Hajebrahimi, B. Poorali, M. Pahlevani, P.K. Jain, and A. Bakhshai, "A Supervisory Control System for Nanogrids Operating in the Stand-Alone Mode, IEEE Transactions on Power Electronics, Volume: 36, Issue: 3, pp. 2914 – 2931, March 2021

[3] A. David, J. Maire, and M. Dessoude, "Influence of voltage dips and sags charteristics on electrical machines and drives," the 3rd inter. Conf. on power quality PQA94, no. 1B-1.31, The Netherlands, 1994.

[4] Snehal Bagawade, Iman Askarian, Majid Pahlevani, and Praveen Jain, "A New Discrete Four Quadrant Control Technique for Grid-Connected Full-Bridge AC–DC Converters," IEEE Journal of Emerging and Selected Topics in Power Electronics, (Early Access) DOI: 10.1109/JESTPE.2021.3088878, 14 June 2021.

[5] Priyanka E. Bhaskaran a, C. Maheswari, S. Thangavel, M. Ponnibala, T. Kalavathidevi, and N.S. Sivakumar, "IoT Based monitoring and control of fluid transportation using machine learning", Elsevier Computer and Electrical Engineering Journal, no. 89, 2021.

[6] A. R. Abu'lWafa, "Industrial load management in Egypt," the 11th proc. of inter. Assoc. of Science and Technology for Development (IASTED): Modeling, Identification, and Control, pp. 267-268, Austria, 1992.

[7] O. S. Ebrahim and P. K. Jain "LQR-based Stator Field Oriented Control for the Induction Motor Drives," *the23rd IEEE Applied Power Electronic Conf.* (APEC 2008), USA, 2008.

[8] O. S. Ebrahim, M. F. Salem, P. k. Jain, and M. A. Badr, "Application of linear quadratic regulator theory to the stator field oriented control of induction motors" IET Electr. Power Appl., 2010, Vol. 4, Iss. 8, pp. 637–646.

[9] O. S. Ebrahim, A. S.Elgendy, M. A. Badr, and P. K. Jain, "ANN-Based Optimal Energy Control of Induction Motor in Pumping Applications," IEEE Trans. on Energy Conversion, No.3.1, Oct. 2010.

[10] K. Warwick, "Neural networks for systems and control," the 11th proc. of inter. Assoc. of Science and Technology for Development (IASTED): Modeling, Identification, and Control, pp. 7-10, Austria, 1992.

[11] A. Wald, "Sequential analysis", Dover New York, 1947. (book)

[12] The European commission efficiency regulations (EU) 2019/1781: For low voltage electric motors and variable speed drives.

[13] Ian Miller, "Fluid Couplings vs VFDs for High Inertia Rotating Driven Loads: A Selection Guide Reviewing the Merits of Both Options," Power Transmission Engineering, pp.44-46, 2017.

[14] M. G. Say, "Alternating Current Machines", John Wiley & Sons, 5th edition, 1968, (book).

[15] K. Smith and S. Jain, "The necessity and challenges of modeling and coordinating microprocessor based thermal overload functions for device protection," The 70 Annual Conference for Protective Relay Engineers (CPRE), 2017.

[16] P. K. Jain; G. Nishith, "Digital State Control with Preview for a Shunt Active Filter Having the Function of Active Rectifier", *The 33rd Ann. Conf.of the IEEE Industrial Electronics Society* (IECON'07), 2007, Taiwan.

[17] O. S. Ebrahim, K. O. Shawky, M. A. Badr, and P. K. Jain " An Induction Motor Drive System with Intelligent Supervisory Control for Water Networks Including Storage Tank," *World Academy of Science, Engineering and Technology,* Inter. Journal of Mechanical and Industrial Eng., Vol:17, No:3, 2023.

Osama S. Ebrahim received his BSc (Hons), MSc, and PhD degrees from Ain Shams University, Egypt, in 1993, 1998 and *2004* respectively. Since 2005, he has been Assistant Professor in the Electrical Power and Machines Department, Ain Shams University, and has served as a consultant engineer for the Electrical and Mechanical Research Institute, National Water Research Center, Egypt, where he provides scientific guidance in developing energy efficient and environmentally friendly variable speed pumping units. He has pursued research activities as a postdoctoral fellow at the Centre for Energy and Power Electronics Research (ePOWER), Queen's University, Canada, in 2006 and since 2008, with grant funding from the Ontario Ministry of Research and Innovation. Dr. Ebrahim is a member of IEEE and of the Egyptian Syndicate of Engineering. he wasa Treasurer of the IEEE Kingston Section, Canada in 1 applications to power electronic converters, automatic voltage regulators, sensorless motor drives, wind alternators and solar PV systems. 2008. His research interests include modern control theories and their digital applications.

Kareem O. Shawky is a student at the Civil Dept., Faculty of Engineering, Ain Shams University, Egypt. His research interest includes smart cities, building and hydro storage systems and networks, traffic management and control and intelligent cloud computing.

Praveen K. Jain (S'86, M'88, SM'91, F'02) received a BE (Hons.) degree from the University of Allahabad, India, and MASc and PhD degrees from the University of Toronto, Canada, in 1980, 1984, and 1987, respectively, all in electrical engineering.

Presently, he is a Professor and Tier-1 Canada Research Chair in Power Electronics at Queen's University in Kingston, Ontario, Canada. He is also the founding Director of the Queen's Centre for Energy and Power Electronics Research (ePOWER).

From 1994 to 2000, Dr. Jain was a Professor at Concordia University, Montreal, Canada, where was engaged in teaching and research in the field of power electronics. Prior to this (1989-1994) he was a Technical Advisor with the Power Group, Nortel Networks, Ottawa, Canada, where he was providing guidance for research and development of advanced power technologies for telecommunications. During 1987-1989, he was with Canadian Astronautics Ltd., Ottawa, Canada, where he played a key role in the design and development of high frequency power conversion equipment for the Space Station Freedom. He was a design engineer and production engineer at Brown Boveri Company and Crompton Greaves Ltd., India, respectively during the period of 1980-1981. He also has considerable consulting experience with the industry including Astec, Ballard, General Electric, Intel and Nortel.

Dr. Jain has attracted over $20M funding to conduct research and establish the state-of-the-art Energy and Power Electronics Applied Research Laboratory (ePEARL) at Queen's University. He has also supervised over 75 research engineers, postdoctoral fellows and graduate students. He has considerable experience in transferring technology from university lab to practical product designs. He secured over $35M venture funding to found CHiL Semiconductor to design and market mixed analog/digital semiconductor chip products. Dr. Jain has published over 375 publications including 40 patents in the area of power electronics. Dr. Jain is a Fellow of the Institute of Electrical and Electronics Engineering (FIEEE), a Fellow of the Engineering Institute of Canada (FEIC) and a Fellow of the Canadian Academy of Engineering (FCAE). He is also the recipient of 2004 Engineering Medal (R&D) of the Professional Engineers of Ontario. He is an Associate Editor of IEEE Transactions on Power Electronics, and KIPE Journal of Power Electronics. Recently, Dr. Jain has been awarded the 2021 IEEE Medal in Power Engineering.

Mohamad A. Badr received the BSc (Hons.) degree from Cairo University, Egypt, MSc degree from Ain-Shams University, Egypt, MASc and PhD degrees from University of Saskatchewan, Canada in 1965, 1969, 1971, and 1974, respectively. He is a Professor in the Electrical Power and Machines Department, Ain-Shams University since 1986.Currently, he is a chairman in the Egyptian Supreme Council for promoting faculty staff members to higher ranks and Dean of Faculty of Engineering and Technology, Future University, Egypt.

Dr. Badr has a considerable contribution in developing the electrical and environmental engineering in Egypt and Saudi Arabia where he directed many conferences, workshops, consultant units and held various teaching positions. Dr. Badr is awarded the Egyptian State Encouraging Award in Engineering Sciences in 1997 and nominated for the UNESCO science prize for outstanding contribution to the scientific development of a member state or region. He is also obtained the Egyptian State Award for Scientific Superiority in Engineering Sciences in 2004. His domain of research activities in the electrical power and machine applications includes interdisciplinary varieties and he published more than 100 conference and Journal papers and three scientific books.